Evaluation of scattered radiation in a radiotherapy treatment for prostate cancer using proton therapy compared to IMRT: a study using the Monte Carlo method

Arthur S B Z Alves[1], Ariadny T Machado[2], Douglas A A Xavier[2], José W P[2],Carla J Santos[2], Lucio P Neves[1,2], Walmir Belinato[3],Ana P Perini[1,2], and William S Santos[1,2]

[1] Physics Institute, Federal University of Uberlândia (INFIS/UFU), Uberlândia, 38408-100, Brazil
[2] Postgraduate Program in Biomedical Engineering (PPGEB/UFU), Electrical Engineering Faculty, Federal University of Uberlândia, Uberlândia, 38400-902, Brazil
[3] Federal Institute of Bahia (IFBA), Vitória da Conquista, 48030-220, Brazil

Correspondent author: arthur.zuchetti@ufu.br

Abstract. Radiotherapy using proton beams, or proton therapy, represents a major advance in the field of radiotherapy and clinical research. It delivers the prescribed dose in a precise manner and causes little to no damage to nearby structures. The main source of scattered radiation to the rest of the body in this case, comes from the creation of secondary particles, mainly neutrons, due to the high energies used in this beam. Using the Monte Carlo method with an anthropomorphic voxel phantom object, this paper compared the dosimetric data obtained from a prostate cancer treatment simulation using proton therapy, with the results previously obtained from literature for a similar treatment using photon beams. The deposited neutrons doses throughout the whole body were lower than IMRT by about 49%. In the irradiation field and in the organs nearby the tumor, the neutron's absorbed dose was less than half the photon dose, while in the remaining vital organs, disregarding those in the target area, the dose of neutrons exceeded IMRT by more than threefold. However, this last set of organs away from the fields, still represents less than 10% of the whole-body scattered absorbed dose contribution in IMRT and 16% in proton therapy.

Keywords: radiotherapy; proton therapy; prostate cancer, Monte Carlo method.

1. Introduction

Data on the incidence of prostate cancer cases show that in recent decades, Brazil has been the country with the highest rate of this neoplasm, with about 200 cases per 100,000 inhabitants per year, effectively being tied only with the United States [1].

This scenario creates great scientific interest in research areas that aim at less invasive means of treating this sensitive region. Advanced radiotherapy treatments, such as Intensity Modulated Radiotherapy (IMRT), have sought to reduce the dose rate delivered to healthy tissues, however, dosimetric calculations still indicate that there is a high exposure of regions such as the bladder, femur, and rectum [2].

The alternative that has been showing promise in terms of reducing exposure in healthy tissues, is radiotherapy with heavy particle beams, such as protons. The also called proton therapy, can deposit a much lower entry dose into the tissues when compared to radiotherapy with light particles such as photons and electrons, in addition to having a narrow peak of dose deposition (called "Bragg Peak"), and having no exit dose, creating a punctual exposure area [3].

A convenient way to quantify this dose comparison is through computational simulation data, using the Monte Carlo method (MMC). From the Monte Carlo N-Particle® Transport Code System Version 6.2 (MCNP6.2) [4] is possible to simulate anatomies and treatments, considering the stochastic nature of radiation transport.

This work compares the dosimetric information of a prostate cancer radiotherapy with photons, to one with protons. Relating literature data with those obtained in simulations, using the code MCNP6.2 for the results referring to proton therapy.

2. Material and Methods

2.1 Determination of conversion factors for absorbed dose and risk of induced cancer

Direct determination of doses to patient organs and tissues during radiotherapy procedures is a complicated process for most situations. In the literature, is common to express the results of doses in organs and tissues through the ratio between an estimated or measured dosimetric quantity by another quantity that can be obtained more easily through experimental arrangements. The result of this ratio is called the dose conversion factor (CF) [5, 6, 7], which is a function of the field and source parameters (field size, field position, focus distance skin, etc.) and the anatomical properties of the anthropomorphic phantom, such as the elemental composition of the relevant body tissues and the applied radiation transport method. Thus, measurements performed in dosimetry can be interpreted in terms of absorbed dose, multiplying the value obtained from the instrument by the appropriate CF for exposure situations like the actual exposure. For consistency, in this research, the estimated absorbed doses in the target and non-target organs of the anthropomorphic phantom were presented in this format.

2.2 MCNP6.2 radiation transport code

Monte Carlo simulations were performed using the MCNP6.2 code. This code makes it possible to model the environment, physical processes, and complex and heterogeneous geometries, being ideal for use in primary and secondary dose calculations, seeking to reproduce reality.

In this study, the ICRP 110 reference adult computational anthropomorphic phantom [8] was used to anatomically represent the patient submitted to proton therapy for prostate cancer. Table 1 presents the main anthropometric information of the phantom that will be used during the Monte Carlo simulation process to estimate doses in organs. For a more accurate evaluation of the doses, it was necessary to remove the phantom arms, as they were in the main beam line.

Table 1. Some main properties of the ICRP 110 reference voxel-based anthropomorphic phantom [8].

Characteristics	
Height (m)	1,76
Mass (kg)	73,0
Z voxel dimension (mm)	8,0
X and Y voxel dimension (mm)	2,137
Voxel volume (mm^3)	36,54
X axis voxel number	254
Y axis voxel number	127
Z axis voxel number	222
Tissue voxels number	1.950.255
Empty voxels number	5.211.021
Total voxel number	7.161.276

2.3 Proton beam accelerator nozzle modeling

Figure 1 shows the path taken by the proton beam from its origin to the irradiated target [9]. The beam generated by the particle accelerator is transported to the treatment room where the patient is positioned. The width of the beam created is in the order of millimeters and, therefore, it must be spread out to treat tumors of any size. The system used in this research will be double scattering, which produces a uniform and large area proton treatment beam.

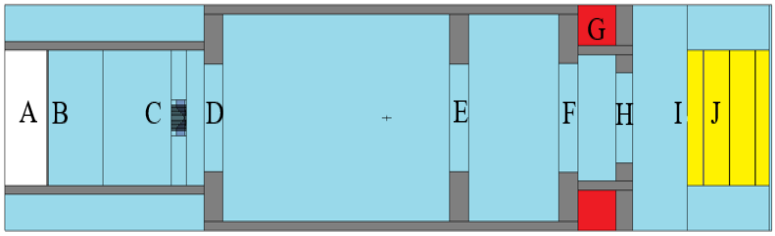

Figure 1. View of the particle accelerator nozzle with double dispersion: (A) proton input beam in a vacuum, (B) range modulation wheel (polycarbonate), (C) scatterer (lead), (D) structural support, (E) pre-collimator, (F) base for nozzle, (G) concrete wall of the treatment room, (H) nozzle, (I) final opening and (J) irradiated object.

The output structure consists of the input of the accelerated beam which is, first, in vacuum (A). Next, the beam passes through the dual scattering system composed of components (B) and (C) to spread the thin beam of protons over a wider region of maximum dose, being useful for a variety of shapes and sizes of protons. tumors, also known as “Spread Out Braggs Peak (SOBP)”. Components (D) and (E) are used to eliminate protons with a high scattering angle, also providing support for the nozzle (F). Finally, the nozzle, or final opening, is composed of components (G), (H), and (I), serving to determine the shape of the final cross-section of the treatment field

The proton source was modeled as a parallel beam of protons with a Gaussian initial energy distribution with a mean energy of 250 MeV, defined in the SDEF card of the MCNP6.2 code. In this research, the doses of primary protons radiation and secondary photons radiation and neutrons were not considered. For all simulations, the number of simulated particles was 1E+9 to obtain statistical uncertainties associated with the simulations within an acceptable limit, which is below 1% [4].

3. Results

The simulation was performed based on the planned treatment for the irradiation of a tumor located in the prostate. This dose was distributed in two beams incident bilaterally in the sagittal plane, precisely in the target area of the patient. Figure 2 illustrates the procedure in a color map with the intensity of the secondary neutron dose in each region.

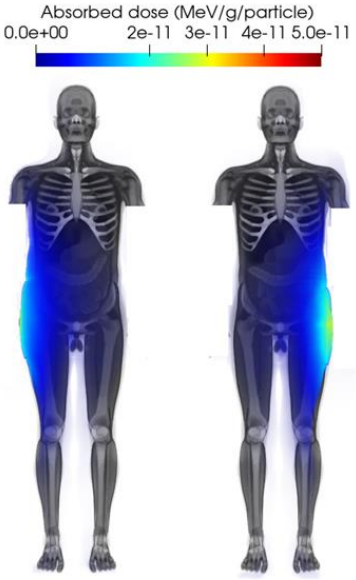

Figure 2. Calculated neutron absorbed dose distributions for the left lateral (LL), and right lateral (RL) field.

From these data, it was calculated the neutron absorbed dose in each of the interest organs from the phantom, with their due uncertainties. These doses are organized in Table 2, being classified by the incision side of the beam and by the total dose in the tissues.

Table 2. Equivalent dose per absorbed dose Sv/Gy (H/D) obtained from the proton treatment simulation. Values for the left lateral field (LL) and right lateral field (RL) of the beam, and the sum of both, all with their respective percentage uncertainties.

Organ	LL Beam Dose	LL Error (%)	RL Beam Dose	RL Error (%)	Total M/D (LL+RL)	Total H/D error (LL+RL) (%)
Stomach	7.66E-03	0.52	8.22E-03	0.52	1.59E-02	1.04
Colon	6.21E-03	0.26	6.63E-03	0.26	1.28E-02	0.52
Liver	2.35E-03	0.55	2.51E-03	0.55	4.86E-03	1.10
Lungs	3.39E-04	0.46	3.59E-04	0.47	6.97E-04	0.93
Esophagus	1.66E-03	1.90	1.76E-03	1.88	3.42E-03	3.78
Pancreas	5.11E-03	0.91	5.39E-03	0.91	1.05E-02	1.82
Brain	2.35E-04	1.93	2.45E-04	1.94	4.81E-04	3.87
Bone marrow	5.13E-04	0.18	5.46E-04	0.18	1.06E-03	0.36
Small intestine	1.25E-02	0.25	1.33E-02	0.25	2.59E-02	0.50
Spleen	7.38E-03	0.81	7.84E-03	0.81	1.52E-02	1.62
Gall bladder	2.97E-03	1.64	3.07E-03	1.60	6.04E-03	3.24
Heart	2.91E-03	0.69	3.10E-03	0.69	6.02E-03	1.38
Lymph nodes	1.38E-03	0.31	1.47E-03	0.30	2.86E-03	0.61
Kidneys	1.06E-03	0.61	1.11E-03	0.61	2.18E-03	1.22

Thyroid	8.53E-04	3.90	8.78E-04	3.98	1.73E-03	7.88
Testes	6.45E-03	0.91	6.89E-03	0.97	1.33E-02	1.88
Bladder	1.32E-02	0.59	1.41E-02	0.59	2.73E-02	1.18
Bone surface	2.19E-04	0.17	2.33E-04	0.17	4.53E-04	0.34
Ureter	4.71E-03	0.98	4.92E-03	0.90	9.63E-03	1.88
Spinal cord	1.57E-03	1.77	1.64E-03	1.75	3.21E-03	3.52
Salivary glands	3.04E-04	2.49	3.35E-04	2.44	6.39E-04	4.93
Adrenal	2.07E-03	1.64	2.23E-03	1.64	4.29E-03	3.28
Skin	4.08E-03	0.06	4.34E-03	0.06	8.42E-03	0.12
Prostate	1.23E-02	1.97	1.32E-02	1.23	2.56E-02	3.20
Rectum	1.00E-01	1.82	1.09E-01	2.09	2.09E-01	3.91
Other tissues	4.04E-04	0.07	4.29E-04	0.07	8.33E-04	0.14

4. Discussions

Looking at Table 1, it is noted that the organs adjacent to the irradiation target region are those with the highest H/D values. Since they are directly on the path between the accelerator and the target, these regions are more susceptible to exposure to secondary neutrons generated in this path. Similarly, regions further from the tumor, such as the upper part of the trunk and head organs, tend to receive a lower dose than the rest of the body.

As a comparison parameter, it is possible to look at conventional radiotherapy treatment techniques with photon beams. IMRT (Intensity Modulated Radiotherapy) is known to be one of the most modern techniques for this treatment modality, as it presents a dose delivery accuracy and protection of organs at risk greater than other similar techniques, such as Conventional 3D Radiotherapy [10].

From the dosimetric results of the simulations involving the IMRT technique in the treatment of prostate cancer found in the literature [11] and the results simulated in this work, a direct comparative analysis of the H/D values obtained in both cases can be performed, since the phantom object is the same.

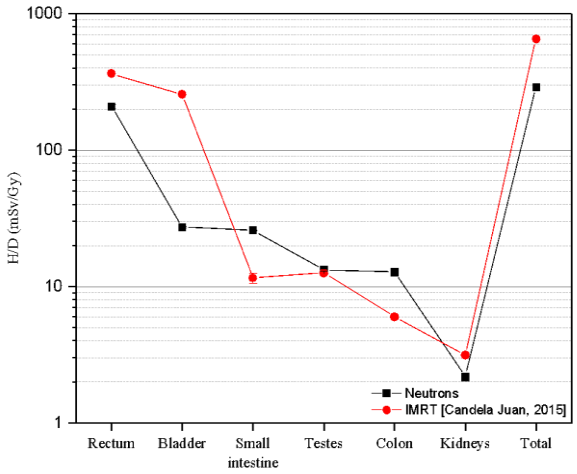

Figure 3. Equivalent dose per absorbed dose (H/D) for organs adjacent to the treatment target, comparing data from (Candela Juan, 2015) for the same treatment using IMRT with those obtained in this work for secondary neutrons.

As described in Figure 3, the results of radiation scattered to healthy adjacent organs and tissues in the case of IMRT present an absolute value considerably higher than in the simulation of the same treatment, using the proton beam. This difference can be explained by the fact that photons have a more superficial dose deposition, while protons manage to apply the prescribed dose almost punctually, causing less exposure of healthy structures close to the tumor. It is noteworthy that for the dose values of this work, only the secondary neutrons generated in the treatment were considered, which are not the only secondary particles formed, however, are responsible for the greater contribution of radiation scattered during the procedure.

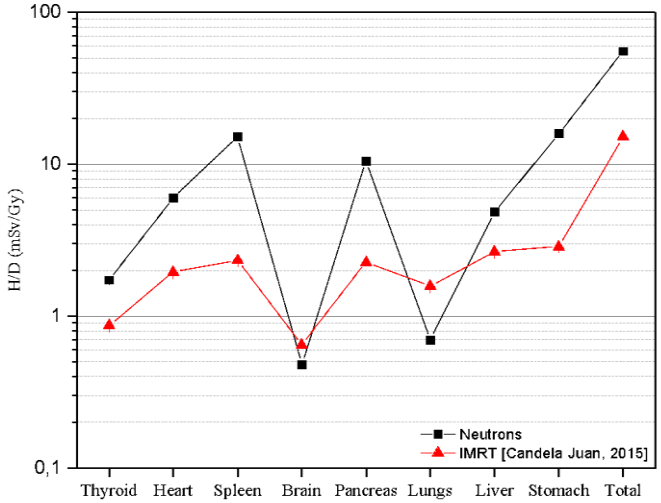

Figure 4. Equivalent dose per absorbed dose (H/D) for vital organs away from the treatment target, comparing data from [Candela Juan, 2015] for the same treatment using IMRT with those obtained in this work for secondary neutrons.

Analogously, this comparison is also valid for the furthest organs from the treatment target, as shown in Figure 4. This time it is noticeable that the H/D values are lower in the IMRT technique, this is mainly because it uses several beams with smaller energies, which decreases the cross section for photonuclear effects and, consequently, decreases the secondary radiation generated in the path of the beam. And, as this radiation is responsible for most of the dose to organs far from the irradiation field, proton therapy has a higher H/D value. However, in absolute values of whole-body equivalent dose, IMRT still has higher dose values than proton therapy.

5. Conclusions

From the comparison between the results of this work, simulating a treatment of prostate cancer with protons, and data from the literature for the same treatment with photons, it is observed that for organs immediately in the treatment field path, the deposited radiation by the photons was shown to have a much greater contribution to the dose than the neutrons generated by the proton beam. However, for organs outside this field, in the upper part of the trunk and head, the contribution of secondary neutrons presented a higher dose than scattered photons and secondary particles generated in the IMRT technique.

In summary, although photons show a high deposition of entrance and exit dose in the irradiated field area, they do not contribute as much as neutrons to the dose in furthest organs and tissues, which indicates that the generated neutrons will represent a dose deposition more homogeneous throughout the entire body, while photons have a more punctual deposition in the treatment region. It should be noted

that considering a whole-body dose, proton therapy still showed an exposure approximately 2.3 times lower than the IMRT technique for an equivalent treatment.

6. References

[1] Cindy Ke Zhou, David P. Check, Joannie Lortet-Tieulent, Mathieu Laversanne, Ahmedin Jemal, Jacques Ferlay, Freddie Bray, Michael B. Cook, Susan S. Devesa. Prostate cancer incidence in 43 populations worldwide: an analysis of time trends overall and by age group. International journal of cancer, v. **138**, n. 6, p. 1388-1400, 2016.

[2] Luxton, Gary; HANCOCK, Steven L.; BOYER, Arthur L. Dosimetry and radiobiologic model comparison of IMRT and 3D conformal radiotherapy in treatment of carcinoma of the prostate. International Journal of Radiation Oncology* Biology* Physics, v. **59**, n. 1, p. 267-284, 2004.

[3] Lourenço. D. F. Monte Carlo simulations and analysis of experimental data of a clinical proton therapy system using adaptive aperture. Disponível em: <https://catalogo-ist.biblioteca.ulisboa.pt/cgi-bin/koha/opac-detail.pl?biblionumber=641021>. Acesso em: 4 fev. 2023

[4] Werner, C. J. MCNP Users Manual-Code Version 6.2. Los Alamos National Laboratory, Los Alamos, 2017.

[5] ICRP 116. International Commission on Radiological Protection: ICRP Publication 116, Conversion Coefficients for Radiological Protection Quantities for External Radiation Exposures. Annals of the ICRP, v. **40**(2-5), 2010.

[6] Mehrdad Shahmohammadi Beni, C. Y. P. Ng, D. Krstic, D. Nikezic, K. N. Yu. Conversion coefficients for determination of dispersed photon dose during radiotherapy: NRUrad input code for MCNP. PLoS ONE., v. **12**, 2017.

[7] Fontenot, J., Newhauser, W. D., Titt, U. Design tools for próton therapy nozzles based on the double-scattering foil technique. Radiat. Prot. Domim., v. **116**, 1-4, 2005.

[8] ICRP 110. International Commission on Radiological Protection: ICRP Publication 110, Adult Reference Computational Phantoms. Annals of the ICRP, v. **39**(2), 2009.

[9] Delaney, T. F., Kooy, H. M. Proton and charged particle radiotherapy. Philidelphia, PA: Lippincott Williams and Wilkins, 2008.

[10] Erjona Bakiu, Ervis Telhaj, Elvisa Kozma, Ferdinand Ruçi, Partizan Malkaj. Comparison of 3D CRT and IMRT tratment plans. Acta Informatica Medica, v. **21**, n. 3, p. 211, 2013.

[11] Candela Juan, Cristian. Radiation protection of patients undergoing high-dose-rate brachytherapy: peripheral dose estimation, review of radiation risks and implant shielding design. 2015.

Acknowledgement

The authors would like to thank the Brazilian agencies: CNPq (314520/2020-1 (L.P.N), 312124/2021-0 (A.P.P) and 309675/2021-9 (W.S.S); UNIVERSAL Project (407493/2021-2); INCT Project (406303/2022-3) and MAI/DAI Project (403556/2020-1)) and FAPEMIG Projects (APQ-02934-15, APQ-03049-15 e APQ-04215-22).